Available online at www.sciencedirect.com
SCIENCE DIRECT®
International Journal of Non-Linear Mechanics 40 (2005) 395–409
INTERNATIONAL JOURNAL OF NON-LINEAR MECHANICS
www.elsevier.com/locate/nlm

Peridynamic modeling of membranes and fibers

S.A. Silling[a,*], F. Bobaru[b]

[a] *Computational Physics Department, MS-0378, Sandia National Laboratories, Albuquerque, NM 87185-0378, USA*
[b] *Department of Engineering Mechanics, University of Nebraska – Lincoln, W317.6 Nebraska Hall, Lincoln, NE 68588, USA*

Received 30 July 2004; accepted 4 August 2004

Abstract

The peridynamic theory of continuum mechanics allows damage, fracture, and long-range forces to be treated as natural components of the deformation of a material. In this paper, the peridynamic approach is applied to small thickness two- and one-dimensional structures. For membranes, a constitutive model is described appropriate for rubbery sheets that can form cracks. This model is used to perform numerical simulations of the stretching and dynamic tearing of membranes. A similar approach is applied to one-dimensional string like structures that undergrow stretching, bending, and failure. Long-range forces similar to van der Waals interactions at the nanoscale influence the equilibrium configurations of these structures, how they deform, and possibly self-assembly.

Keywords: Elasticity; Membranes; Dynamic fracture; Rubber

1. Introduction

The classical theory of solid mechanics, because it relies on partial differential equations, contains inherent limitations when applied to problems involving failure of materials: since the spatial derivatives do not exist on crack tips or surfaces, the differential equations cannot be applied directly on these singularities. The traditional way of working around this issue is through the special techniques that have been developed in the field of fracture mechanics. These special techniques are not always satisfactory, either physically or mathematically, in part because of the need for supplemental relations that control crack growth (for example, crack growth velocity as a function of stress intensity factor). In the present work, an alternative approach is pursued, which is to reformulate the fundamental equations of continuum mechanics in such a way that they can be applied regardless of whether a discontinuity occurs as a result of deformation. This alternative approach is called the *peridynamic* model [1,2]. The peridynamic model uses integral rather differential equations, so the mathematical structure does not break down when a discontinuity occurs. Instead, fracture is treated as

* Corresponding author.
E-mail address: sasilli@sandia.gov (S.A. Silling).

0020-7462/$ - see front matter © 2004 Elsevier Ltd. All rights reserved.
doi:10.1016/j.ijnonlinmec.2004.08.004

a natural outcome of deformation that emerges according to the equations of motion and constitutive model. Consequently, simulation of fracture growth within the peridynamic model does not require supplemental kinetic relations that, in traditional fracture mechanics, would be needed to determine crack initiation, growth velocity, direction, arrest, branching, and other features. Another aspect of the peridynamic model that makes it attractive for certain applications, particularly at the nanoscale, is that long-range forces, such as intermolecular and surface forces, can be incorporated easily as part of the constitutive model. This is because the model treats all forces between particles in a continuum as though they act across a finite distance, in contrast with the fundamental assumption in the classical theory that all forces internal to a body result from contact. The purpose of this paper is to discuss the properties of the peridynamic model for simulating the deformation, interaction, and failure of thin two- and one-dimensional structures. After briefly reviewing the full three-dimensional theory, a peridynamic model is described for elastic sheets that can undergo damage and fracture. This model is applied to the tearing of sheets and to the dynamic fracture of a stretched membrane. The theory is then further specialized to stringlike structures, similar to long molecules, that sustain tensile loads while interacting with each other through intermolecular and contact forces.

2. Peridynamic theory

The peridynamic theory may be thought of as a continuum version of molecular dynamics. The acceleration of any particle at $\mathbf{x}$ in the reference configuration at time t is found from the equation of motion,

$$\rho\ddot{\mathbf{u}}(\mathbf{x},t) = \int_{\mathscr{H}_{\mathbf{x}}} \mathbf{f}(\mathbf{u}(\mathbf{x}',t)-\mathbf{u}(\mathbf{x},t),\mathbf{x}'-\mathbf{x})\,\mathrm{d}V_{\mathbf{x}'} + \mathbf{b}(\mathbf{x},t), \tag{1}$$

where $\mathscr{H}_{\mathbf{x}}$ is a neighborhood of $\mathbf{x}$, $\mathbf{u}$ is the displacement vector field, $\mathbf{b}$ is a prescribed body force density field, ρ is mass density in the reference configuration, and $\mathbf{f}$ is a *pairwise force function* whose value is the force vector (per unit volume squared) that the particle $\mathbf{x}'$ exerts on the particle $\mathbf{x}$. In the following discussion, we denote the relative position of these two particles in the reference configuration by $\boldsymbol{\xi}$ and their relative displacement by $\boldsymbol{\eta}$:

$$\boldsymbol{\xi} = \mathbf{x}' - \mathbf{x}, \quad \boldsymbol{\eta} = \mathbf{u}(\mathbf{x}',t) - \mathbf{u}(\mathbf{x},t). \tag{2}$$

Using these definitions, $\boldsymbol{\eta}+\boldsymbol{\xi}$ represents the *current* relative position vector between the particles. The direct physical interaction (which occurs through unspecified means) between the particles at $\mathbf{x}$ and $\mathbf{x}'$ will be called a *bond*. The concept of a bond that extends over a finite distance is a fundamental difference between the peridynamic theory and the classical theory, which is based on the idea of contact forces (interactions between particles that are in direct contact with each other). It is convenient to assume that for a given material there is a positive number δ, called the *horizon*, such that

$$|\boldsymbol{\xi}| > \delta \implies \mathbf{f}(\boldsymbol{\eta},\boldsymbol{\xi}) = \mathbf{0} \quad \forall\boldsymbol{\eta}. \tag{3}$$

For the remainder of this discussion, $\mathscr{H}_{\mathbf{x}}$ will denote the spherical neighborhood of $\mathbf{x}$ in $\mathscr{R}$ with radius δ (Fig. 1). A material is said to be *microelastic* if the pairwise force function is derivable from a scalar *micropotential* w:

$$\mathbf{f}(\boldsymbol{\eta},\boldsymbol{\xi}) = \frac{\partial w}{\partial \boldsymbol{\eta}}(\boldsymbol{\eta},\boldsymbol{\xi}) \quad \forall\boldsymbol{\xi},\boldsymbol{\eta}. \tag{4}$$

The micropotential is the strain energy in a single bond and has dimensions of energy per unit volume squared. The energy per unit volume in the body at a given point (i.e., the local strain energy density) is therefore found from

$$W = \frac{1}{2}\int_{\mathscr{H}_{\mathbf{x}}} w(\boldsymbol{\eta},\boldsymbol{\xi})\,\mathrm{d}V_{\xi}. \tag{5}$$

The factor of $1/2$ appears because each endpoint of a bond "owns" only half the energy in the bond. If a body is composed of a microelastic material, work done on it by external forces is stored in recoverable form in much the same way as in the classical theory of elasticity. Furthermore, it can be shown that the micropotential depends on the relative displacement vector $\boldsymbol{\eta}$ only through the *scalar* distance between the deformed points. Thus, there is a scalar-valued function $\hat{w}$ such that

$$\hat{w}(y,\boldsymbol{\xi}) = w(\boldsymbol{\eta},\boldsymbol{\xi}) \quad \forall\boldsymbol{\xi},\boldsymbol{\eta}, \quad y = |\boldsymbol{\eta}+\boldsymbol{\xi}|. \tag{6}$$

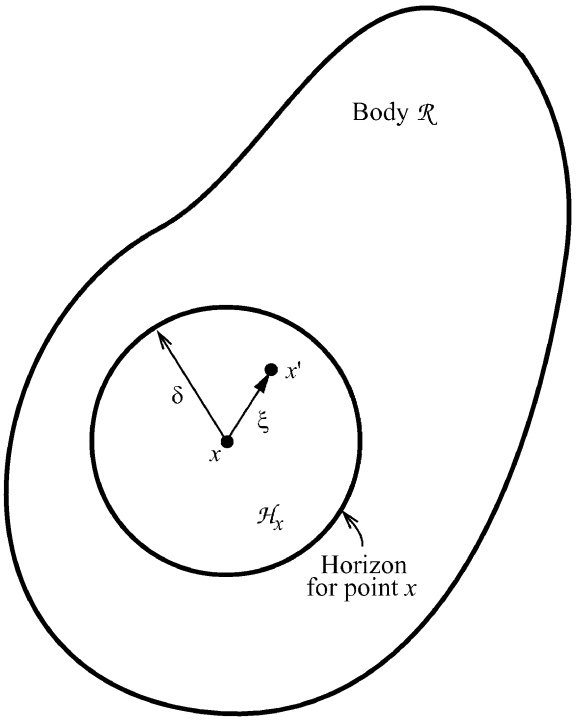

Fig. 1. Each point $\mathbf{x}$ in the body interacts directly with points in the sphere $\mathcal{H}_\mathbf{x}$ through *bonds*.

Therefore, the interaction between any two points in a microelastic material may be thought of as an elastic (and possibly non-linear) spring. The spring properties may depend on the separation vector $\boldsymbol{\xi}$ in the reference configuration; the material is isotropic if $\hat{w}$ is independent of the *direction* of $\boldsymbol{\xi}$. Combining (4) and (6) and differentiating the latter with respect to the components of $\boldsymbol{\eta}$ leads to

$$\mathbf{f}(\boldsymbol{\eta}, \boldsymbol{\xi}) = \frac{\boldsymbol{\xi} + \boldsymbol{\eta}}{y} \hat{f}(y, \boldsymbol{\xi}), \quad y = |\boldsymbol{\xi} + \boldsymbol{\eta}| \quad \forall \boldsymbol{\xi}, \boldsymbol{\eta}, \tag{7}$$

where $\hat{f}$ is the scalar-valued function defined by

$$\hat{f}(y, \boldsymbol{\xi}) = \frac{\partial \hat{w}}{\partial y}(y, \boldsymbol{\xi}) \quad \forall y, \boldsymbol{\xi}. \tag{8}$$

Eq. (7) shows that the force vector in a bond is parallel to the current relative position vector between the two particles. It also shows that the force vector exerted by any particle $\mathbf{x}'$ on $\mathbf{x}$ equals minus the force vector that $\mathbf{x}$ exerts on $\mathbf{x}'$. Conservation of angular and linear momenta is therefore automatically satisfied by a microelastic material model. Also, since $\hat{w}$ is invariant with respect to rigid rotation of a bond, the requirement of objectivity is trivially satisfied. The function $\hat{f}$ in (8) explicitly contains $\boldsymbol{\xi}$ because internal forces within a solid body depend not just on the relative position of particles in the *deformed* configuration, but also on their relative position in the *reference* configuration. (This, of course, is true in the classical theory as well as the peridynamic theory.) However, for the modeling of long-range forces, such as van der Waals forces, the positions of particles in the reference configuration are not usually important. So, for these types of forces, the scalar interparticle force $\hat{f}$ can be assumed to have no explicit dependence on $\boldsymbol{\xi}$ but dependence only on the deformed interparticle distance y. For example, later in this paper, material models with the following form will be used:

$$\hat{w}(y, \boldsymbol{\xi}) = \hat{w}_1(y, |\boldsymbol{\xi}|) + \hat{w}_2(y). \tag{9}$$

Here, w_1 represents the solid behavior of the material, while w_2 models the long-range forces. These two terms can have different horizons, i.e., the long-range interactions may be exist at distances beyond the horizon for solid interactions.

Damage may be incorporated into a peridynamic constitutive model by allowing the bonds for solid interactions to break irreversibly. The simplest assumption is that this breakage occurs when a bond is extended beyond some predetermined critical bond deformed length. Since the breakage is irreversible, time and position must now be included as arguments in the interparticle force, for example

$$\bar{f}(y, \boldsymbol{\xi}, \mathbf{x}, t) = \hat{f}(y, \boldsymbol{\xi}) \mu(\boldsymbol{\xi}, \mathbf{x}, t), \tag{10}$$

where μ is a history-dependent scalar-valued function that takes on values of either 1 or 0:

$$\mu(\boldsymbol{\xi}, \mathbf{x}, t) = \begin{cases} 1 & \text{if } y(\boldsymbol{\xi}, \mathbf{x}, t) < y_0 \text{ for all } 0 \leqslant t' \leqslant t, \\ 0 & \text{otherwise,} \end{cases} \tag{11}$$

where y_0 is the critical value of bond deformed length for breakage. (y_0 may depend on reference bond length $|\boldsymbol{\xi}|$.) Recall that any particle in the continuum has an infinite number of bonds connecting it to other particles. During deformation, some of these bonds may break as determined by (11), and breakage of the bonds occurs independently among different bond lengths

and orientations $\boldsymbol{\xi}$ for a given particle. In practice, bond breakage in a peridynamic body usually evolves in such a way as to form two-dimensional surfaces. These surfaces correspond to cracks; their growth is the way fracture propagation occurs spontaneously in the peridynamic theory. The initiation and growth process occurs without reference to any supplemental kinetic relation that controls crack growth on the basis of a stress intensity factor or similar quantity. In this sense, fracture modeling in the peridynamic theory is "autonomous" and represents a fundamental difference between the present theory and the techniques of traditional fracture mechanics.

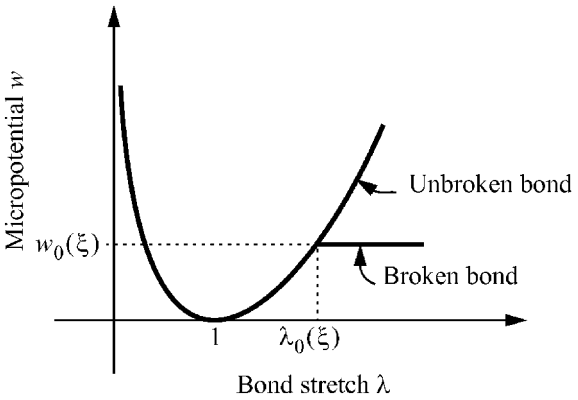

Fig. 2. Micropotential (strain energy in a bond per unit volume squared) as a function of bond stretch.

3. Membranes

The finite deformation of elastic membranes has a long history of experimental study [3–5]. The applications of membrane mechanics continue to grow and are evident in such diverse fields as biomechanics, for example [6]; and thin films and nanostructures, for example [7,8]. The theory of elastic membrane deformation similarly has been fertile ground for the development of new and important mathematical and computational techniques related to the modeling of large deformations including wrinkling, dynamics, stability, rupture, and fracture, such as in [9–14], among many others. Similarly, the study of fibers, including networks of fibers, from a continuum mechanics point of view is gaining importance in the molecular biology, cell biology, and nanoscience communities, concurrently with ab initio and molecular dynamics methods of analysis [15–18]. With a view toward investigating the relevance of the peridynamic model to these phenomena, the three-dimensional theory outlined in the previous section will now be specialized to two-dimensional membranes, and in Section 6, to fibers. Here, a *membrane* means a body that is sufficiently thin that its resistance to bending is very low. To specialize (1) to membranes, it is necessary merely to change the volume integrals to area integrals:

$$\rho\ddot{\mathbf{u}}(\mathbf{x},t) = h\int_{\mathscr{H}_{\mathbf{x}}} \mathbf{f}(\mathbf{u}(\mathbf{x}',t)-\mathbf{u}(\mathbf{x},t),\mathbf{x}'-\mathbf{x})\,\mathrm{d}A_{\mathbf{x}'} + \mathbf{b}(\mathbf{x},t), \tag{12}$$

where h is the thickness of the membrane (in the reference configuration) and $\mathrm{d}A_{\mathbf{x}'}$ is a differential area of the membrane at the point $\mathbf{x}'$ in the reference configuration. All other variables in (12) have the same meanings and dimensions as in the full three-dimensional expression (1). However, because the membrane lacks bonds that extend to particles off of the surface, a given $\mathbf{f}$ will result in different bulk material response when used in (12) than in (1). Displacements are permitted in any direction, including normal to the surface. It is not assumed that the membrane is flat in the reference configuration. h is assumed constant for present purposes, but the theory is easily generalized to variable thickness membranes. As a prototype material model for an isotropic rubbery membrane, consider the following micropotential:

$$\hat{w}(y,\boldsymbol{\xi}) = w(\lambda,|\boldsymbol{\xi}|) = c(\lambda^2+1/\lambda^2-2)\ g(|\boldsymbol{\xi}|), \quad 0<|\boldsymbol{\xi}|\leqslant\delta, \tag{13}$$

where c is a positive constant, g is a scalar-valued function, and λ is the bond *stretch* defined by

$$\lambda = y/|\boldsymbol{\xi}|, \quad y = |\boldsymbol{\eta}+\boldsymbol{\xi}|. \tag{14}$$

This micropotential function is graphed in Fig. 2. From (8) and (14), it follows that the interparticle force

corresponding to (13) is

$$\hat{f}(y,\boldsymbol{\xi}) = \frac{\partial \hat{w}}{\partial y} = \frac{\mathrm{d}w}{\mathrm{d}\lambda}\frac{\mathrm{d}\lambda}{\mathrm{d}y} = \frac{2c}{|\boldsymbol{\xi}|}(\lambda - 1/\lambda^3)\ g(|\boldsymbol{\xi}|), \quad 0 < |\boldsymbol{\xi}| \leqslant \delta. \tag{15}$$

The function g is included mainly for completeness: its meaning is that bonds with different *reference* lengths can have different elastic response. In practice, g has little effect except with regard to deformations that occur on a length scale smaller than the horizon. For example, the wave dispersion properties of the material at small wavelengths are affected by terms of this type [1].

There is a parallel between the present notion of a constitutive model in the peridynamic theory and models for rubbery materials that have been developed in the classical theory involving networks of molecular chains [19]. Each point in a peridynamic body is connected to many other points through microelastic bonds whose energy as a function of stretch is prescribed; the bulk properties of the solid follow from the properties of this bond energy. The same is basically true of molecular chains in the rubber models, so there is an analogy between these molecular chains and peridynamic bonds. Along the same lines, various alterations of (13) may be made to introduce hardening response at large stretches [20] due to limits in chain extensibility [21,22], for example a power-law model of the form

$$w_n(\lambda) = [c(\lambda^2 + 1/\lambda^2) + c'\lambda^n]\ g(|\boldsymbol{\xi}|) \tag{16}$$

may be useful where c' and n are constants, $n > 1$.

It will now be demonstrated that the peridynamic membrane model given in (13) coincides with a reasonable *classical* elastic material, at least for purposes of homogeneous deformations. To do this, consider a homogeneous deformation of a peridynamic membrane and let $\mathbf{F} = \mathbf{1} + \nabla\mathbf{u}$ be the usual deformation gradient tensor. Without loss of generality, assume that in some Cartesian coordinate system the components of $\mathbf{F}$ are given by

$$[\mathbf{F}] = \begin{bmatrix} \lambda_1 & 0 \\ 0 & \lambda_2 \end{bmatrix}, \tag{17}$$

where λ_1 and λ_2 are the principal stretches. The bulk response will be determined by finding the strain energy $W(\mathbf{F})$ per unit volume contained in all the peridynamic bonds connected to any point $\mathbf{x}$ in the body. The bond stretch is now found from (14),

$$\lambda = \frac{|\mathbf{F}\boldsymbol{\xi}|}{|\boldsymbol{\xi}|} = \sqrt{\lambda_1^2\cos^2\theta + \lambda_2^2\sin^2\theta}, \tag{18}$$

where the polar coordinates of $\boldsymbol{\xi}$ are $\xi = |\boldsymbol{\xi}|$, $\xi_1 = \xi\cos\theta$, and $\xi_2 = \xi\sin\theta$. Combining this with (5) and (13) and carrying out the integrations leads to

$$W(\mathbf{F}) = \frac{h}{2}\int_0^{\delta}\int_0^{2\pi} w(\lambda(\theta),\xi)\,\xi\,\mathrm{d}\theta\,\mathrm{d}\xi = \frac{\pi hcR}{2}\left(\lambda_1^2 + \lambda_2^2 + \frac{2}{\lambda_1\lambda_2} - 4\right) \tag{19}$$

where

$$R = \int_0^{\delta} \xi\, g(\xi)\,\mathrm{d}\xi. \tag{20}$$

The macroscopic strain energy density W in (19) depends only on the principal stretches and is symmetric with respect to interchange of these stretches, $\lambda_1 \longleftrightarrow \lambda_2$. Further, it can be shown that (19), although it does not explicitly include any out-of-plane stretch λ_3, is obtainable from the three-dimensional elastic material given by

$$W = \frac{\pi hcR}{2}\left(\lambda_1^2 + \lambda_2^2 + \lambda_3^2 + \frac{1}{\lambda_1^2\lambda_2^2\lambda_3^2} - 4\right) \tag{21}$$

under the requirement that the out-of-plane stress component σ_{33} vanish. The material specified in (21) is a special case of the Blatz–Ko material, a standard constitutive model for compressible materials like foam rubber [23].

4. Membranes with damage

At this point damage can be introduced into the material model for this elastic membrane by setting a critical stretch for bond breakage. Following (10), (15) is replaced by

$$\bar{f}(y,\boldsymbol{\xi},\mathbf{x},t) = \frac{2c}{|\boldsymbol{\xi}|}(\lambda - 1/\lambda^3)\ g(|\boldsymbol{\xi}|)\ \mu(\boldsymbol{\xi},\mathbf{x},t), \quad 0 < |\boldsymbol{\xi}| \leqslant \delta, \tag{22}$$

where μ is defined by (11) such that bonds break when their deformed length equals $y_0 = |\boldsymbol{\xi}|\lambda_0$, where λ_0

is a critical bond stretch for failure. For the moment, λ_0 will be assumed constant, although possible dependence on $|\boldsymbol{\xi}|$ will be introduced later. Now consider the bulk response of this material when damage is included. Suppose the membrane is subjected to a time-dependent *homogeneous* deformation such that λ_1 and λ_2 are non-decreasing and, for simplicity, $\lambda_1 \geqslant \lambda_2$ for all t. First, it is necessary to determine which bonds have broken as a function of the current principal stretches. From (18), the directions θ of broken bonds are found from the condition

$$\lambda_0^2 \leqslant \lambda_1^2 \cos^2\theta + \lambda_2^2 \sin^2\theta. \tag{23}$$

Hence broken bonds occupy the wedges

$$|\theta| \leqslant \theta_0(\lambda_1, \lambda_2) \quad \text{and} \quad |\theta - \pi| \leqslant \theta_0(\lambda_1, \lambda_2), \tag{24}$$

where

$$\theta_0(\lambda_1, \lambda_2) = \sin^{-1}\sqrt{\frac{\lambda_1^2 - \lambda_0^2}{\lambda_1^2 - \lambda_2^2}}, \qquad 1 \leqslant \lambda_2 \leqslant \lambda_0 \leqslant \lambda_1. \tag{25}$$

Let $w_0(\xi)$ denote the strain energy in a bond of initial length ξ when it breaks. By (13), this is

$$w_0(\xi) = c(\lambda_0^2 + 1/\lambda_0^2 - 2)\ g(|\boldsymbol{\xi}|). \tag{26}$$

Now compute the strain energy remaining in the body as it stretches, accounting for broken bonds. For accounting purposes, it is assumed that the strain energy in broken bonds equals the strain energy at the time they broke (see Fig. 2). So, to find the current energy density, the integral in the first of (19) becomes

$$\bar{W}(\mathbf{F}) = 2h \int_0^\delta \left\{ w_0(\xi)\ \theta_0(\lambda_1, \lambda_2) + \int_{\theta_0(\lambda_1,\lambda_2)}^{\pi/2} w(\lambda(\theta), \xi)\, \mathrm{d}\theta \right\} \xi\, \mathrm{d}\xi, \tag{27}$$

where $\lambda(\theta)$ is supplied by (18). The term on the left within the braces represents the contribution of the broken bonds, while the term on the right is for the unbroken bonds. Carrying out the integrations in (27) leads to

$$\bar{W}(\mathbf{F}) = 2hcR\left[\left(\lambda_0^2 + \frac{1}{\lambda_0^2}\right)\theta_0 + \left(\lambda_1^2 + \lambda_2^2\right) \times \left(\frac{\pi}{4} - \frac{\theta_0}{2}\right) + \frac{\sin 2\theta_0}{4}(\lambda_2^2 - \lambda_1^2) + \frac{1}{\lambda_1\lambda_2}\tan^{-1}\left(\frac{\lambda_1}{\lambda_2}\cot\theta_0\right) - \pi \right], \tag{28}$$

where R is defined in (20). In the case of zero damage ($\theta_0 \equiv 0$), (28) reduces to (19). The corresponding Piola stress component σ_{11} as a function of λ_1 is shown in curves (b) and (c) in Fig. 3. The two curves are for different (but constant) transverse stretch λ_2.

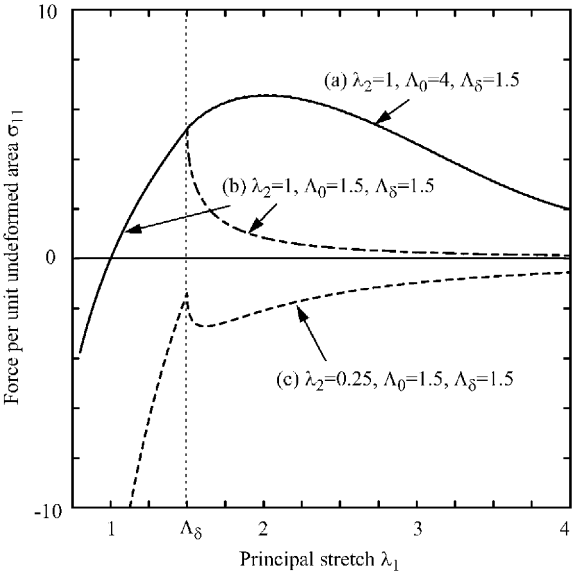

Fig. 3. Force per unit undeformed area as a function of bond stretch in a membrane for three combinations of damage parameters and transverse stretch. In all three cases damage initiates when the membrane is stretched to $\lambda_1 = \Lambda_\delta$.

Just as the bond elastic properties can depend on their reference length (through $g(\xi)$), the bond critical stretch can also depend on this length. For example, the following two-parameter family of critical bond stretches allow longer bonds to fail either before or after shorter ones in a homogeneous deformation, depending on the

choice of parameters:

$$\lambda_0(\xi) = \Lambda_0 + (\Lambda_\delta - \Lambda_0)\xi/\delta, \quad 0 < \xi \leqslant \delta, \tag{29}$$

where Λ_0 and Λ_δ are positive constants representing the critical values of bond stretch at $\xi = 0$ and at $\xi = \delta$, respectively. A variety of damage-related phenomena may be exhibited in the bulk response of this family of materials, as illustrated in Fig. 3. As the three curves in the figure illustrate, depending on the damage properties and transverse stretch, the stress may reach a global maximum at a plateau or a cusp, or a local maximum followed by a further increase. Additional flexibility in the model can be obtained by allowing the critical bond stretch to depend on other quantities, such as time, rate of stretch, external fields, and damage at nearby points.

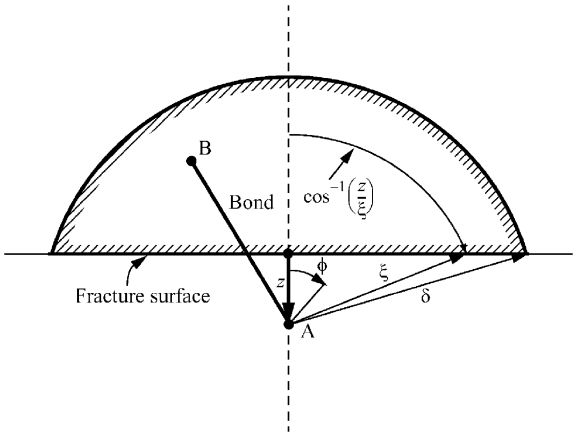

Fig. 4. Computation of energy release rate in Eq. (30) by summation of the work required to break bonds, such as the line segment AB, that initially connected the two sides separated by the crack.

5. Crack growth in membranes

The analysis at the end of the previous section assumes that the deformation remains homogeneous while the stretches are varied, but in an initial value problem non-homogeneities such as phase boundaries or localizations would be expected from such a material. Also, any pre-existing defect in the membrane would be expected to strongly influence the way in which failure would occur. Homogeneous deformations therefore tell only part of the story with regard to material failure, and from the point of view of the peridynamic theory this is one of the less interesting parts. Of greater interest is the possibility of fracture and the conditions under which it can occur in a membrane composed of this material. Recall that damage occurs at the level of an individual bond, and each material particle is connected to an infinite number of its neighbors by such bonds. The energy requirement to advance an existing crack in a peridynamic membrane will now be computed. To break an individual bond requires an amount of work $w_0(\xi)$ per unit volume squared, where this work is permitted to depend on initial bond length through dependence on $g(\xi)$ and on some bond breakage model such as (29). The work required to pull apart two portions of a membrane across a crack surface is therefore the sum, per unit crack area, of all the bonds that initially connected one portion of the membrane to the other. Referring to Fig. 4, this quantity is given by

$$G = 2h \int_0^\delta \int_z^\delta \int_0^{\cos^{-1}(z/\xi)} w_0(\xi)\, \xi \, \mathrm{d}\phi \, \mathrm{d}\xi \, \mathrm{d}z, \tag{30}$$

where w_0 is defined in (26). The significance of this result is that if a crack is present in a deforming body, then it is possible that the energy G needed to extend a crack according to (30) is less than what is required to deform the body further at constant crack length according to (5). This situation makes it energetically favorable for the crack to grow, and is simply a restatement of the Griffith energy criterion for crack growth. The difference in the peridynamic approach is that any crack growth, when the conditions are right, occurs spontaneously as a result of the equation of motion and the constitutive model.

6. Fibers and long-range forces

To model fibers of constant cross-sectional area A, the appropriate equation of motion is

$$\rho \ddot{\mathbf{u}}(\mathbf{x}, t) = A \int_{\mathscr{H}_\mathbf{x}} \mathbf{f}(\mathbf{u}(\mathbf{x}', t) - \mathbf{u}(\mathbf{x}, t), \mathbf{x}' - \mathbf{x})\, \mathrm{d}s_{\mathbf{x}'} + \mathbf{b}(\mathbf{x}, t), \tag{31}$$

where $\mathrm{d}s_{\mathbf{x}'}$ is a differential path length along the fiber at the point $\mathbf{x}'$ in the reference configuration and all

other variables have the same meanings and dimensions as in (1). It is not assumed that the fiber is straight in the reference configuration. Allowing for interaction between fibers (and between different points on the same fiber), the constitutive model is of the form (9),

$$\hat{w}(y, \boldsymbol{\xi}) = w_1(\lambda, \xi) + w_2(y), \tag{32}$$

where λ is still defined by (14). The term w_1 describes the solid-like response of the fiber, while w_2 describes the interactions through long-range forces (that are independent of $\boldsymbol{\xi}$). Thus, w_2 depends only on the *current* distance between two particles, not on their initial positions. Therefore, a reasonable prototype material model for a fiber is

$$\begin{aligned} w_1(\lambda, \xi) &= c\left(\lambda^2 + \frac{1}{\lambda^2} - 2\right)\ g(\xi), \\ w_2(y) &= \alpha\left(\frac{a}{y}\right)^{12} - \beta\left(\frac{a}{y}\right)^{6}, \end{aligned} \tag{33}$$

where a, α, β, and c are positive constants; a represents a characteristic length for the long-range interactions. This particular choice of w_2 has the form of a 6-12 van der Waals potential, but many other alternative forms are possible. Because of the strongly singular nature of the van der Waals force as two particles are brought close together, it does not make sense to apply this force to mutually interacting "neighboring" particles in a continuous body. On the other hand, it can be applied to interactions between the particles of two separated continuous bodies, a fact that is exploited in analyzing the physics of surfaces [24]. In the peridynamic model, this notion of long-range interaction between separate bodies (or possibly separate parts of the same body) is conveniently included by permitting the long-range forces to discriminate between particles along the fibers. Thus, the coefficients in the van der Waals terms vary according to the particle pairs, i.e., $\alpha(\mathbf{x}, \mathbf{x}')$ and $\beta(\mathbf{x}, \mathbf{x}')$, provided the dependence of these functions satisfies the conservation of linear momentum requirement

$$\alpha(\mathbf{x}, \mathbf{x}') = \alpha(\mathbf{x}', \mathbf{x}) \quad \text{and} \quad \beta(\mathbf{x}, \mathbf{x}') = \beta(\mathbf{x}', \mathbf{x}). \tag{34}$$

The pairwise force function for the fiber follows from (7), (14), and (33),

$$\begin{aligned} \mathbf{f} &= \left[\frac{1}{|\boldsymbol{\xi}|}\frac{\partial w_1}{\partial \lambda} + \frac{\mathrm{d}w_2}{\mathrm{d}y}\right]\mathbf{m} \\ &= \left[\frac{2c}{|\boldsymbol{\xi}|}\left(\lambda - \frac{1}{\lambda^3}\right)\ g(\xi) - \frac{12\alpha}{a}\left(\frac{a}{y}\right)^{13} \right. \\ &\quad \left. + \frac{6\beta}{a}\left(\frac{a}{y}\right)^{7}\right]\mathbf{m}, \\ \mathbf{m} &= \frac{\boldsymbol{\xi} + \boldsymbol{\eta}}{y}, \quad y = |\boldsymbol{\eta} + \boldsymbol{\xi}|, \quad \lambda = y/|\boldsymbol{\xi}|. \end{aligned} \tag{35}$$

The concept of damage in the peridynamic sense applies only to the solid-like interactions, so damage in the fiber is incorporated as

$$\begin{aligned} \bar{\mathbf{f}} = &\left[\frac{2c}{|\boldsymbol{\xi}|}\left(\lambda - \frac{1}{\lambda^3}\right)\ g(\xi)\ \mu - \frac{12\alpha}{a}\left(\frac{a}{y}\right)^{13}\right. \\ &\left. + \frac{6\beta}{a}\left(\frac{a}{y}\right)^{7}\right]\mathbf{m}, \end{aligned} \tag{36}$$

where μ has the same definition as before, given by (11). To compute the energy per unit area G required to create an isolated fracture in the fiber due to stretching, the bond breakage energies w_0 are summed across the crack surface:

$$G = A\int_0^{\delta}\int_z^{\delta} w_0(\xi)\,\mathrm{d}\xi\,\mathrm{d}z. \tag{37}$$

Solid-like connections between fibers (cross-links) are easily included in the formulation by defining peridynamic bonds between them in the reference configuration. The work required to break these cross-linked connections can be evaluated by summing up their respective w_0 as illustrated above for the case of a break within a single fiber. The work required to overcome any long-range forces between two fibers initially in contact with each other would also be included in this calculation.

7. Examples

This section presents some examples of predictions of membrane and fiber deformation and failure according to the theory discussed above. Because it is based

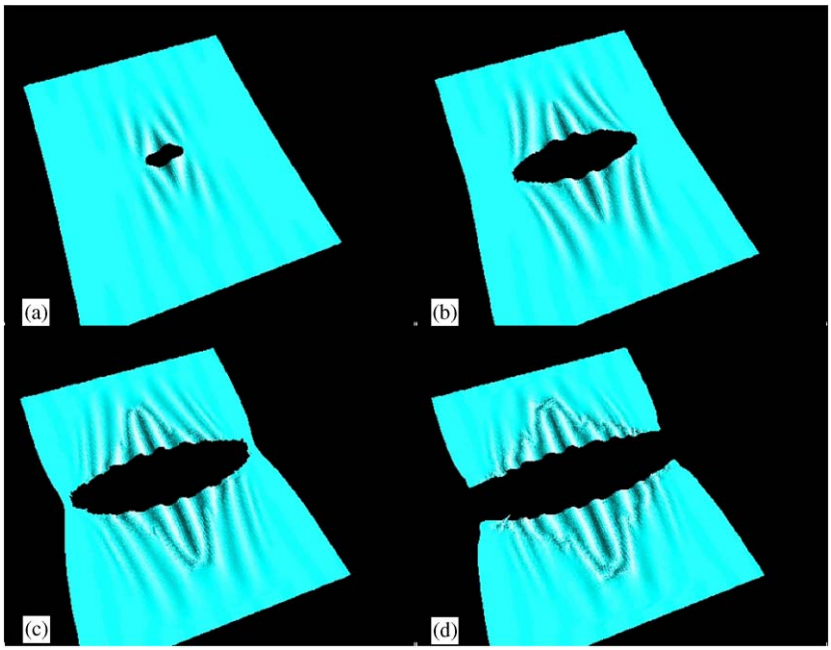

Fig. 5. (a–d) Tensile loading of a membrane containing a slit, showing transition to dynamic fracture (Example 1).

on integral equations, which are less amenable to exact solutions than PDEs in initial value problems, all of the present results were obtained using a numerical solution method. The numerical method itself is described elsewhere [25]; it relies on a straightforward approximation of the integral in (1) by a finite sum arising from discretization of the continuous body into nodes. It will also be shown in work to be documented separately that in the ideal case of a uniform grid with spacing Δx, the error in this approximation is of order Δx^2.

7.1. Dynamic growth of a single crack from a defect

In problem 1, a square elastic membrane of thickness 0.5 mm and side length 50 mm contains a narrow slit of length 10 mm. The edges of the membrane parallel to the slit are pulled apart, creating mode I loading at the tips of the slit. The other two edges are free. The membrane is represented using the constitutive and damage models discussed above with properties corresponding to a longitudinal wave speed of 1000 m/s and a mass density of 1200 kg/m^3. The critical bond stretch for failure is $\lambda_0 = 2$. The membrane is free in the transverse (through the thickness) direction at all points other than the clamped ends. The slit is created in the numerical model by breaking all the peridynamic bonds that intersect the slit anywhere along its length. In this way, a uniform numerical grid may be used without any special grid generation method in the vicinity of the damaged region of the membrane. Fig. 5 shows how the slit evolves into a dynamic crack at four different times. In view (a), the slit has not yet started to grow. Wrinkles are visible along the slit edges. The wrinkles are "seeded" using small initial displacements that vary sinusoidally throughout the numerical model. Otherwise, these wrinkles occur spontaneously. The wrinkles occur because the membrane is free along the edges normal to the slit and therefore tends to develop compressive strains parallel to the slit. In the remaining views in Fig. 5, the crack is propagating. Wrinkles appear in the wake of the crack. In view (d), the crack has grown to the free edges of the membrane, and the two resulting halves of the membrane are rebounding. In Fig. 6, the predicted crack growth velocity is plotted as a function of crack tip position. The increase in crack velocity up to an asymptotic limiting value (in this case about

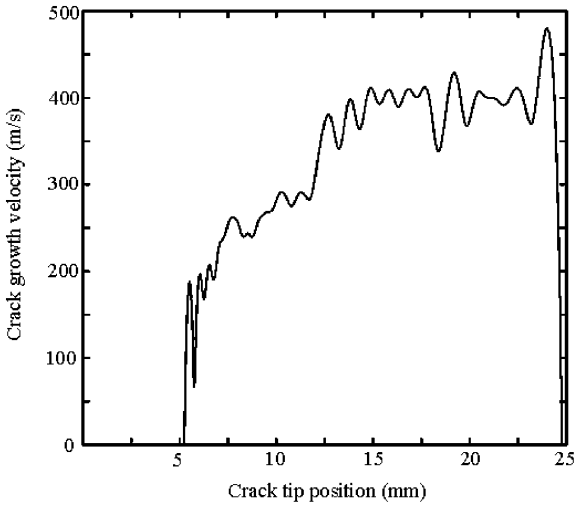

Fig. 6. Crack growth velocity in a membrane as a function of crack tip position (Example 1).

400 m/s), as well as oscillations in the velocity, are characteristic of dynamic fracture in brittle solids (see, for example, Fig. 20 in [26]). The value of the limiting velocity in this case is well below the Rayleigh wave speed, which is about 700 m/s, that under ideal conditions is an upper bound for mode I dynamic crack speed [27]. The general features of the static and propagating crack in the peridynamic solution, especially the pronounced blunting, are consistent with results in the classical theory for crack tip singularities and elliptical holes [28–32]. However, physically impossible unbounded strains do not occur in the peridynamic result, and therefore the crack tip fields differ fundamentally from the classical finite elasticity results. (The same is true of crack tip fields in certain other non-local theories[33].)

7.2. Bursting of a balloon

In this problem, a spherical membrane subjected to an internal pressure is struck by a rigid fragment. The resulting damage at the impact point develops into dynamic cracks that grow along the sphere. The unpressurized balloon has density $1200\,\mathrm{kg/m^3}$ and elastic properties corresponding to a bulk modulus of 800 MPa. The critical stretch for failure is $\lambda_0 = 1.75$. The radius of the sphere is 0.1 m and the thickness is 0.0015 m. The internal pressure is 1.5 MPa, resulting in a hoop stress of 50 MPa. Fig. 7 shows the propagation of dynamic fractures from the point of impact around the circumference of the balloon. The cracks are blunt and irregular, and they occasionally release fragments of the membrane. It is not yet known whether these irregularities are indicative of experimentally observed instabilities [34,35] or if they are due to purely numerical effects.

7.3. Tearing of a membrane

In this example, a rectangular membrane is held fixed along three sides. The fourth side is free, except for a segment that is pulled upward (out of the plane) and forward (toward the interior of the membrane) with constant velocity. The membrane has a density of $1200\,\mathrm{kg/m^3}$ and a thickness of 0.5 mm. It is modeled as a brittle microelastic material with a bulk modulus of 300 MPa and a critical stretch to failure $\lambda_0 = 0.1$. Stress concentrations are created at the ends of the segment that is lifted. These stress concentrations eventually nucleate cracks that propagate into the rectangle. The two cracks, when they are nucleated, are mostly in mode III, but as they advance they become mostly mode I. This mode transition occurs because, as the cracks move away from the boundary, the membrane can more easily displace and rotate out of the plane in such a way that the loading near the crack tips becomes tensile. This loading is such that the cracks tend to advance toward each other and eventually intersect, forming a more or less triangular fragment that completely separates from the remainder of the membrane. Fig. 8 shows the predicted result just before the two cracks merge and the triangular section separates. Because of the asymmetry of the boundary condition (the prescribed velocity segment is closer to one rigid boundary than the other), the cracks grow at different speeds and curve as they grow. As the problem progresses, the slower of the cracks starts to be influenced strongly by the free surface created by the faster crack, and it turns sharply toward this free surface. This tendency of initially parallel cracks in a membrane to merge as they advance is familiar to anyone who has unwrapped a packaged CD or a candy bar. It is also of technological interest in predicting damage to thin structures, such as aerospace structures as a result of impact.

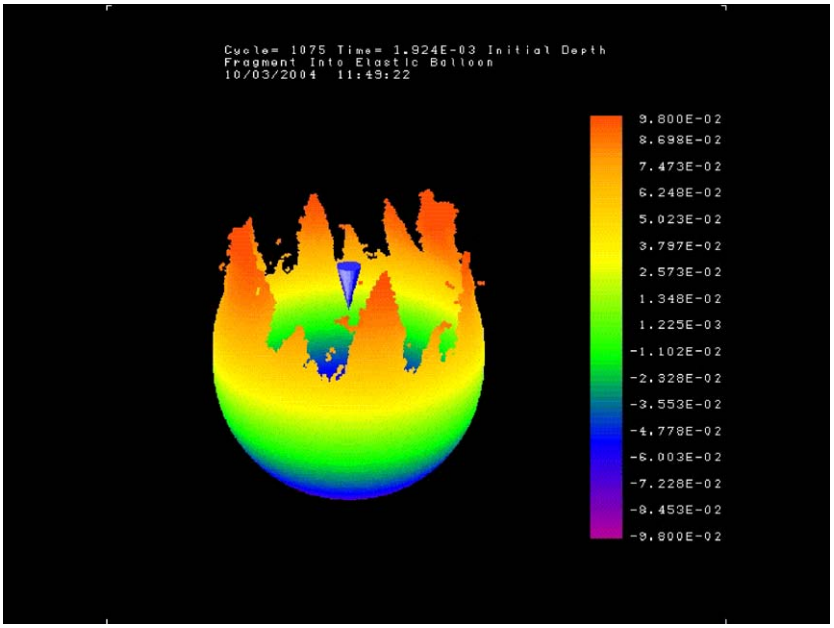

Fig. 7. Simulation of an internally pressurized spherical membrane damaged due to impact of a sharp fragment (Example 2). Shading has no significance other than as an aid to visualization.

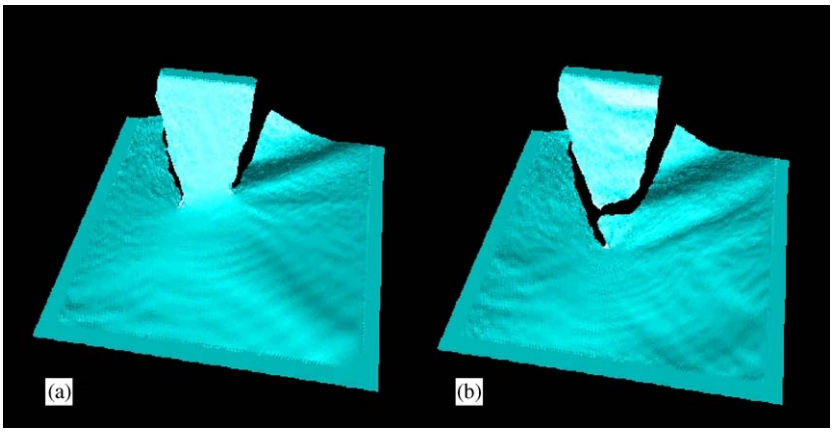

Fig. 8. (a and b) Tearing of a rectangular membrane (Example 3).

7.4. Oscillatory crack path in a membrane

Experimental observations have shown that when a blunt tool is forced through an elastic membrane edge-on, the resulting crack can follow an oscillatory path [36,37]. The reason for these oscillations is not obvious, since intuition would perhaps suggest that a straight crack path would provide the most direct means for the system to reduce its potential energy with no apparent energetic barrier to be overcome. The peridynamic numerical code was applied to this problem as shown in Fig. 9. The membrane is clamped along its long edges and free along its short edges. It has a density of $1200\,\mathrm{kg/m^3}$ and a thickness of

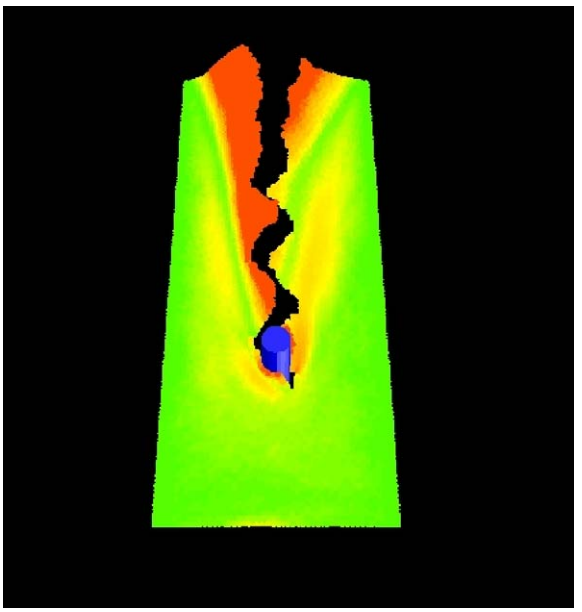

Fig. 9. Oscillatory crack path predicted when a blunt tool is forced through a membrane (Example 4).

0.2 mm. It is modeled as a brittle microelastic material with a bulk modulus of 300 MPa and a critical stretch to failure $\lambda_0 = 0.03$. The blunt tool, in this case a rigid cylinder, starts at the short edge at the rear in the figure. It advances at a constant velocity of 1.0 m/s. The membrane contains a small notch on its rear free surface that serves as an initiation site for a crack. The notch is off-center by a distance equal to the tool radius from the point where the tool first touches the membrane. The asymmetry provided by the notch is crucial in the development of the oscillatory crack path—without it, the straight path is predicted. Also, the oscillations are predicted only when friction between the membrane and the tool is included in the model. (It is not known whether friction is important in the experimental result.) An additional modification to the peridynamic code was required in modeling this problem: the crack tip was permitted to advance only incrementally from its current position at any time. Without this modification, branch cracks tend to form along the crack surface where it rubs against the tool. These spurious branch cracks occur because small perturbations in the numerically predicted crack surface can occasionally act as nucleation sites for new cracks.

The figure shows the predicted crack evolution and the resulting oscillatory crack path. The gross features of this result agree qualitatively with typical experimental results. The oscillations occur in the model because of an interaction between bending and rotation of the membrane out of the plane (which tends to create mode III loading) and stretch within the plane (which tends to create mode I loading) as the tool tries to push folded material out of its way. The predicted amplitude and wavelength of the oscillations are too large compared with the experimental results. These errors occur because the peridynamic model of a membrane tends to resist bending (out of the plane) when the radius of curvature is less than or on the order of the horizon for the material, which in this case was about one half the tool radius. So, the folds that occur in the membrane as it slides up (or down) the tool have too large a radius of curvature, leading to oscillations that are too large.

7.5. Long-range forces within a fiber

Long-range forces play an important role in the shaping of macromolecules such as proteins. In this example, a peridynamic fiber is divided into segments. Each segment attracts the adjacent one through interactions similar to van der Waals forces, while all others repel each other weakly. The fiber has diameter 1.0 nm, a density of 3000 kg/m^3, and microelastic properties corresponding to a bulk modulus of 40 GPa. The segments that attract or repel each other are 7.0 nm in length. The initial shape of the fiber is nearly straight, although it contains small deviations that serve as initiation sites for bending deformation. The fiber spontaneously deforms into the shape shown in the upper plot in Fig. 10, which shows a helix that includes a change in the direction of the chirality near the midpoint of the fiber. It should be noted that because of their highly non-linear nature, systems that interact through long-range forces of this type depend strongly on the history of deformation. Therefore the present results depend to a large extent on the initial conditions.

For a different pattern of attractive and repulsive long-range forces, the lower plot in Fig. 10 is obtained. In this case, two segments near opposite ends of the fiber strongly attract each other, while other segments weakly repel each other. The attracting segments are

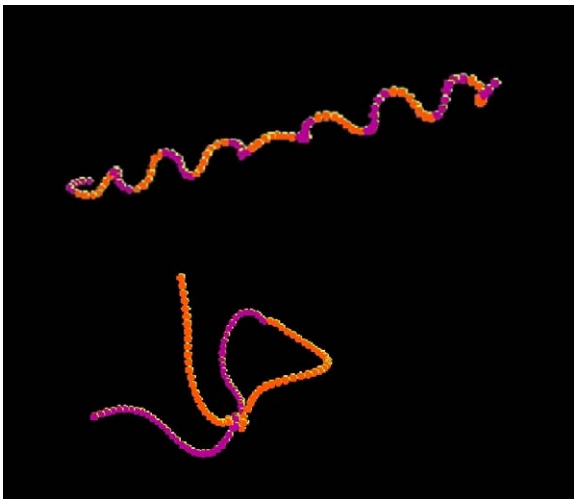

Fig. 10. Fiber deformed by long-range interactions between different parts of the fiber (Example 5).

not only in contact, but partially wind around each other as a means to pull together tightly over as much surface area as possible. Models of this type may prove to be useful in the study of the mechanics of long molecules, which is topic with biological applications such as protein folding and the behavior of DNA, for example [38] and [39].

7.6. Large deformation of a network of fibers

In this example, a square membrane-like network of fibers is stretched from opposite clamped ends. The fibers have a critical bond stretch $\lambda_0 = 0.3$ and a micromodulus corresponding to a Young's modulus of 1.5 GPa. The fibers interact with each other, but not with themselves, through long-range forces similar to van der Waals forces. These interactions influence the deformed shape of the network, which includes cellular patterns, as shown in Fig. 11. Membrane-like networks of electrospun polymer continuous fibers of nanometer scale diameters have been recently produced in the laboratory [40]. It is of importance to analyze the mechanical behavior of such membranes built from randomly oriented fibers or from aligned fibers. In this example we use a model with two families of directional fibers generated inside a box of dimensions 200 nm × 200 nm × 5 nm. In order to mimic manufacturing variability, the fibers of same length have irregular configurations. Locally, the direction of the fiber deviates from the imposed direction (horizontal and vertical in Fig. 11) by means of a Gaussian random distribution with zero mean and standard deviation $\sigma = 0.15$. The starting points for the fibers are also randomly chosen, with a uniform distribution, in narrow regions at the right end and bottom of the membrane in the figure. Fibers that are close enough or in contact with one another are considered perfectly bonded. They interact through peridynamic forces, as well as through long-range forces similar to van der Waals forces. These interactions influence the deformed shape of the network, which includes cellular patterns, as shown in the figure.

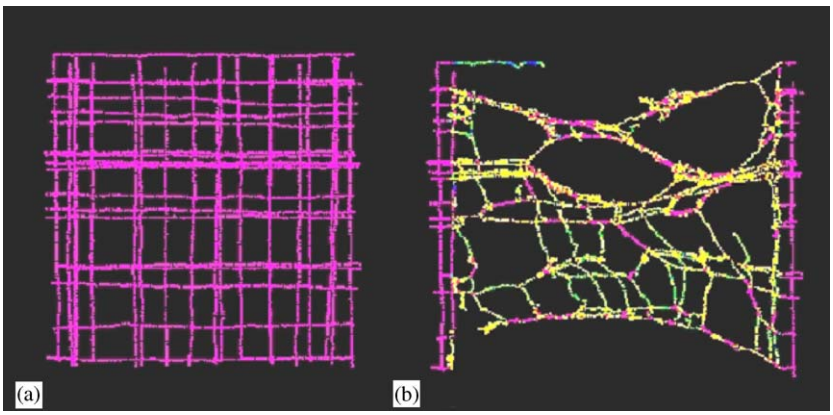

Fig. 11. Stretching of a network of fibers that interact with each other through long-range forces (Example 6). Colors indicate elastic energy. (a) Initial. (b) Deformed.

8. Discussion

Traditional fracture mechanics proceeds from the assumption of a defect within a body and examines the possible growth of the defect based on local conditions. Because in practice all macroscopic structures contain some defect at some size scale, this assumption has served the engineering community well for many years. However, at the nanoscale, it has been demonstrated that it is possible to build structures that are, in effect, perfect or nearly perfect for purposes of mechanics. So, it is perhaps open to question whether traditional fracture mechanics should be applied without modification to nanostructures. The peridynamic model, because it incorporates damage and failure as a natural aspect of deformation, does not require a pre-existing defect to initiate crack growth. It therefore may offer a means to analyze the deformation and failure of nearly perfect materials such as may occur at the nanoscale. At the macroscale, the theory also offers the advantage of "autonomous" crack modeling, in which supplemental relations that control crack evolution are not necessary. For example, there is no need for a relation that governs crack growth speed or direction in terms of a stress intensity factor. The crack growth instead is determined directly as a consequence of the equation of motion and constitutive model. Therefore this approach may allow for arbitrarily complex patterns of growth among multiple, mutually interacting cracks.

Acknowledgements

Sandia is a multiprogram laboratory operated by Sandia Corporation, a Lockheed Martin Company, for the United States Department of Energy's National Nuclear Security Administration under contract DE-AC04-94AL85000. This work was funded by the Department of Energy.

References

[1] S.A. Silling, Reformulation of elasticity theory for discontinuities and long-range forces, J. Mech. Phys. Solids 48 (2000) 175–209.
[2] S.A. Silling, M. Zimmermann, R. Abeyaratne, Deformation of a peridynamic bar, J. Elasticity 73 (2003) 173–190.
[3] L.R.G. Treloar, Physics of Rubber Elasticity, Oxford University Press, Oxford, 1958.
[4] R.S. Rivlin, D.W. Saunders, Large elastic formations of isotropic materials VII: experiments on the deformation of rubber, Philos. Trans. R. Soc. London A 243 (1951) 251–288.
[5] A.N. Gent, P. Marteny, Crack velocities in natural rubber, J. Mater. Sci. 17 (1982) 2955–2960.
[6] G. David, J.D. Humphrey, Further evidence for the dynamic stability of intracranial saccular aneurysms, J. Biomech. 36 (2003) 1143–1150.
[7] J.J. Vlassak, Channel cracking in thin films on substrates of finite thickness, Int. J. Fracture 119 (2003) 299–323.
[8] H.D. Espinosa, B.C. Prorok, Size effects on the mechanical behavior of thin films, J. Mater. Sci. 38 (2003) 4125–4128.
[9] R.W. Ogden, On the stability of asymmetric deformations of a symmetrically-tensioned elastic sheet, Int. J. Eng. Sci. 25 (1987) 1305–1314.
[10] T.E. Tezduyar, L.T. Wheeler, L. Graux, Finite deformation of a circular elastic membrane containing a concentric rigid inclusion, Int. J. Non-Linear Mech. 22 (1987) 61–72.
[11] V.H. Tuzel, H.A. Erbay, The dynamic response of an incompressible non-linearly elastic membrane tube subjected to a dynamic extension, Int. J. Non-Linear Mech. 39 (2004) 515–537.
[12] D.J. Steigmann, A.C. Pipkin, Finite deformations of wrinkled membranes, Quart. J. Mech. Appl. Math. 42 (1989) 427–440.
[13] C.O. Horgan, A.M. Chan, Vibration of inhomogeneous strings, rods, and membranes, J. Sound Vibration 225 (1999) 503–513.
[14] J.A. Blume, Finite dynamic motions of thin rate-dependent sheets, J. Appl. Mech. 57 (1990) 821–827.
[15] P.K. Purohit, J. Kondev, R. Phillips, Force steps during viral DNA packaging, J. Mech. Phys. Solids 51 (2003) 2239–2257.
[16] D. Hennig, J.F.R. Archilla, Stretching and relaxation dynamics in double stranded DNA, Physica A: Stat. Mech. Appl. 331 (2004) 579–601.
[17] D.E. Ingber, Tensegrity I: cell structure and hierarchical systems biology, J. Cell Sci. 116 (2003) 1157–1173.
[18] P. Richard, T. Prasse, J.Y. Cavaille, L. Chazeau, C. Guathier, J. Duchet, Reinforcement of rubbery epoxy by carbon nanofibres, Mater. Sci. Eng. 352 (2003) 344–348.
[19] M.F. Beatty, An average-stretch full-network model for rubber elasticity, J. Elasticity 70 (2003) 65–86.
[20] L.R.G. Treloar, Stress-strain data for vulcanized rubber under various types of deformation, Trans. Faraday Soc. 40 (1944) 59–70.
[21] C.O. Horgan, G. Saccomandi, Constitutive modelling of rubber-like and biological materials with limiting chain extensibility, Math. Mech. Solids 7 (2002) 353–371.
[22] A.N. Gent, A new constitutive relation for rubber, Rubber Chem. Technol. 69 (1996) 59–61.
[23] P.J. Blatz, W.L. Ko, Application of finite elasticity theory to deformation of rubbery materials, Trans. Soc. Rheol. 6 (1962) 223–251.
[24] J. Isrealachvili, Intermolecular and Surface Forces, 2nd ed., Academic Press, London, 1992 (176pp).
[25] S.A. Silling, Dynamic fracture modeling with a meshfree peridynamic code, in: K.J. Bathe (Ed.), Computational Fluid

and Solid Mechanics 2003, Elsevier Science, Amsterdam, 2003, pp. 641–644.
[26] J. Fineberg, M. Marder, Instability in dynamic fracture, Phys. Rep. 313 (1999) 1–108.
[27] E.H. Yoffe, The moving Griffith crack, Philos. Mag. 42 (1951) 739–750.
[28] J.K. Knowles, E. Sternberg, An asymptotic finite-deformation analysis of the elastostatic field near the tip of a crack, J. Elasticity 3 (1973) 67–107.
[29] C.O. Horgan, S.A. Silling, Stress concentration factors in finite anti-plane shear: numerical calculations and analytical estimates, J. Elasticity 18 (1987) 83–91.
[30] P.H. Geubelle, W.G. Knauss, Finite strains at the tip of a crack in a sheet of hyperelastic material: I, homogeneous case, J. Elasticity 35 (1994) 61–98.
[31] K.Ch. Le, H. Stumpf, The singular elastostatic field due to a crack in rubberlike materials, J. Elasticity 32 (1993) 183–222.
[32] A.M. Tarantino, On the finite motions generated by a mode I propagating crack, J. Elasticity 57 (1999) 85–103.
[33] A.C. Eringen, C.G. Speziale, B.S. Kim, Crack-tip problem in non-local elasticity, J. Mech. Phys. Solids 25 (1977) 339–355.
[34] R.D. Deegan, P.J. Petersan, M. Marder, H.L. Swinney, Oscillating fracture paths in rubber, Phys. Rev. Lett. 88 (2002) 014304-1–014304-4.
[35] A. Stevenson, A.G. Thomas, On the bursting of a balloon, J. Phys. D: Appl. Phys. 12 (1979) 2101–2109.
[36] A. Ghatak L. Mahadevan, Crack street: the cycloidal wake of a cylinder tearing through a thin sheet, Phys. Rev. Lett. 91 (2003) 215507-1–215507-4.
[37] B. Roman, P.M. Reis, B. Audoly, S. De Villiers, V. Viguié, D. Vallet, Oscillatory fracture paths in thin elastic sheets, Comptes Rendus Mech. 331 (2003) 811–816.
[38] H.-X. Zhou, Polymer models of protein stability, folding, and interactions, Biochemistry 43 (2004) 2141–2154.
[39] B.D. Coleman, D. Swigon, Theory of supercoiled elastic rings with self-contact and its application to DNA plasmids, J. Elasticity 60 (2000) 173–221.
[40] Y. Dzenis, Y. Wen, Continuous carbon nanofibers for nanofiber composites, Mater. Res. Soc. Symp. Proc. 702 (2002) 173–178.